Received Date : 20-Sep-2016

Revised Date : 09-Oct-2016

Accepted Date : 25-Oct-2016

Article type : Research Letter

Structural characterization of CYP260A1 from *Sorangium cellulosum* to investigate the 1α-hydroxylation of a mineralocorticoid

Yogan Khatri[1], Yvonne Carius[2], Michael Ringle[1], C. Roy D. Lancaster[2] and Rita Bernhardt[1]*

[1]Saarland University, Institute of Biochemistry, Campus B2.2, 66123, Saarbrücken, Germany.

[2]Department of Structural Biology, Institute of Biophysics and Center of Human and Molecular Biology (ZHMB), Faculty of Medicine Building 60, Saarland University, 66421 Homburg, Germany.

***Corresponding author:**

Prof. Dr. Rita Bernhardt

Institute of Biochemistry,

Saarland University,

Campus B 2.2,

D-66123 Saarbruecken, Germany.

Phone: +49 681 302 4241

Fax: +49 681 302 4739

E.mail: ritabern@mx.uni-saarland.de

Highlights:

- Crystal structure of CYP260A1 has been solved.
- CYP260A1 converts 11-deoxycorticosterone into novel steroidal derivatives with 1α-hydroxy-11-deoxycorticosterone as a major product.
- The mutant S326N of CYP260A1 showed higher activity and selectivity for the production of 1α-hydroxy-11-deoxycorticosterone.

Abstract

In this study, we report the crystal structure of the cytochrome P450 CYP260A1 (PDB 5LIV) from the myxobacterium *Sorangium cellulosum* So ce56. In addition, we investigated the hydroxylation of 11-deoxycorticosterone by CYP260A1 by reconstituting the enzyme with the surrogate redox partners adrenodoxin and adrenodoxin reductase. The major product of this steroid conversion was identified as 1α-hydroxy-11-deoxycorticosterone, a novel Δ4 C-21 steroidal derivative. Furthermore, we docked the substrate into the crystal structure and replaced Ser326, the residue responsible for substrate orientation, with asparagine and observed that the mutant S326N displayed higher activity and selectivity for the formation of 1α-hydroxy-11-deoxycorticosterone compared to the wild-type CYP260A1. Thus, our findings highlight the usefulness of the obtained crystal structure of CYP260A1 in identifying biotechnologically more efficient reactions.

Key words:

P450, crystal structure of CYP260A1, mineralocorticoid, S326N, *steroid hydroxylation*

Introduction

Cytochromes P450 (P450s) are heme monoxygenases or the mixed-function oxidases, which can catalyze a number of reactions involved in the metabolism of steroids, fatty acids, drugs, xenobiotics, terpenes and terpenoids [1-7] as well as the late-stage functionalization of several bioactive secondary metabolites [8]. P450s are available in eukaryotes and prokaryotes mainly as multi-component systems and require one or two redox partners for electron transfer from the cofactor NAD(P)H to the heme iron [9].

The attempt of studying P450s to employ them as a biocatalyst for the generation of industrially and pharmaceutically valuable novel biomolecules is considered as a center of attraction for several investigations. Among them, the investigation of steroid hydroxylating P450s is of great interest, because of the pharmaceutical values of the steroidal derivatives. Although 14 human P450s (CYP1B1, CYP7A1, CYP7B1, CYP8B1, CYP11A1, CYPB1, CYP11B2, CYP17A1, CYP19A1, CYP21A2, CYP27A1, CYP39A1, CYP46A1 and CYP51A1) are able to perform physiologically relevant steroid hydroxylation [10], the membrane integrated feature and the low expression level of these P450s hindered their application as biocatalysts. In this regard, bacterial P450s could be the best alternatives. However, there are only few bacterial P450s which can convert steroidal molecules including CYP106A1 [11], CYP106A2 [12, 13], CYP125[14, 15], CYP142 [16], CYP154C5 [17] and CYP260 [18-20].

The myxobacterium *Sorangium cellulosum* So ce56, the producer of the novel cytotoxic compound chevasazole [21] and of catecholate-type siderophores, myxochelins [22], contains 21 P450s [23], 8 ferredoxin and 2 ferredoxin reductases [24]. Among them, CYP260A1 is one of the novel P450s, which we have recently shown to perform a selective 1α-hydroxylation of C-19 steroids [20]. In addition, the oxidation of sesquiterpenes [25] and conversion of drugs [26] by CYP260A1 was also demonstrated. Although its autologous redox partners Fdx2/FdRB and Fdx8/FdRB were identified as efficient for sesquiterpene oxidation [24], the bovine redox partners adrenodoxin (Adx_{4-108}) and adrenodoxin reductase (AdR) were shown to be efficient surrogate redox partners [23], and they were employed for the establishment of an *E. coli* based whole-cell system [27].

In this study, the crystal structure of CYP260A1was solved for the first time, and the conversion of a model Δ4 C21 steroid, 11-deoxycorticosterone (DOC) was investigated. The major product of the DOC conversion by CYP260A1 was purified and identified as 1α-hydroxylated product by 1D- and 2D-NMR analysis, which turned out to be a novel derivative of DOC. In order to investigate the structure-function relationship, DOC was docked into the crystal structure. The residue Ser326, a residue responsible for

positioning the substrate in the active site of CYP260A1, was replaced by asparagine and the conversion of DOC was compared with that of the wild type.

Materials and methods

Molecular cloning, expression and purification of CYP260A1, S326N and other proteins

The heterologous expression and purification of CYP260A1 was performed as described elsewhere [20]. In order to generate the S326N mutant, the CYP260A1 construct was mutated by site directed mutagenesis using primers 5′- aggggatgcgctggtgcccgagc**AA**ctttggcgtgctgcgaatggt -3′ (forward) and 5′-accattcgcagcacgccaaagTTgctcgggcaccagcgcatcccct -3′ (reverse) and a mutagenesis kit (Stratagene Ltd, Cambridge, UK). The correct sequence of the expression construct was confirmed by automated sequencing (MWG, Germany). The mutated protein was expressed and purified as the wild type CYP260A1. The mammalian adrenodoxin reductase, AdR, and truncated adrenodoxin, $Adx_{4–108}$, were expressed and purified as described [28, 29].

Crystallization and structure refinement

CYP260A1 with the highest purity observed by SDS-PAGE and UV-visible spectroscopy analysis was concentrated to 25 mg/ml with a Spin_X UF 50K column (Corning) in 100 mM potassium phosphate buffer (pH 7.4). The screening of the crystallization conditions was performed with 96 well sitting drop vapor diffusion plates of Crystal Screen HT Kit (Hampton Research) at 18°C using the automated crystallization facility at the Department of Structural Biology [30] in the presence and absence of DOC (200 µM).

Non-optimized crystals were obtained with enzyme pre-incubated with DOC (200 µM) in 0.1 MES monohydrate, pH 6.5, containing 1.6 M magnesium sulphate hepthydrate. Different pH values and drop volume ratios were used to optimize the crystallization conditions in 24 well plates using the hanging drop method considering preliminary buffer selection. Reddish crystals used for X-ray diffraction experiments were collected from the same condition at pH 6.8 using equal protein/buffer ratios in the droplets. Crystals with hexagonal shape appeared over a period of two weeks and had dimensions of 230 µM in a diameter. For cryo-protection, crystals were passed through the reservoir solution containing 42% PEG8000 before flash-cooled in liquid nitrogen.

X-ray diffraction data were collected at Beamline ID14-4 from the European Synchrotron Radiation Facility in Grenoble, France, available through the Frankfurt-Homburg Blocked Allocation Group (BAG MX-1303). To define an optimal strategy for data collection, EDNA framework [31] and its automated indexing, cell refinement and strategy calculation were used during data acquisition. All data sets were indexed, integrated and scaled using Mosflm [32] and Scala [33] from the CCP4 program

suite [34]. The CYP260A1 structure was solved by molecular replacement using the chain A of the CYP260B1 (PDB 5HIW) [18] with the program Molrep [35, 36]. Model building was performed with the program COOT [37] and refinement using REFMAC5 [38]. All structural figures were prepared using PyMOL (The PyMOL Molecular Graphics System, Version 1.3 Schrödinger, LLC).

UV-visible absorption spectroscopy

UV-visible spectra for CYP260A1 were measured at room temperature on a double-beam spectrophotometer (UV-2101PC, Shimadzu, Japan). The protein dissolved in 10 mM potassium phosphate buffer, pH 7.4, was used for the spectral measurements of the oxidized and reduced form. The protein was reduced with few grains of sodium dithionite. The active form of CYP260A1 was confirmed by CO-difference spectroscopy using $\Delta\varepsilon_{(450-490)}$ = 91 $mM^{-1}cm^{-1}$according to the method described elsewhere [39].

***In vitro* enzyme activity assay**

The conversion of DOC by the CYP260A1 was carried out with the heterologous electron partners. A protein ratio of CYP260A1: Adx: AdR of 1: 10: 3 was used. The *in vitro* reconstitution assay was performed in a final volume of 250 µl in 20 mM potassium phosphate buffer, pH 7.4. The reaction was started by adding NADPH (1 mM) and incubated for 20 min at 30°C. The reaction was stopped by the addition of 500 µl chloroform and extracted as described [20].

Whole-cell biotransformation using resting cells

The whole-cell biotransformation assay was performed in *E. coli* C43(DE3) cells. The cells were transformed with two plasmids, one for the CYP260A1 and the other one for the redox partners AdR and Adx_{4-108} as described [27]. The seed culture was grown overnight at 37°C in LB-media containing streptomycin (50 µg/ml) and ampicillin (100 µg/ml). The main culture was inoculated with the overnight culture (1:100 dilution) in Terrific broth medium. The expression was induced by adding 1 mM isopropyl β-D-1-thiogalactopyranoside and 0.5 mM 5-aminolevulinic acid at an optical density of 1. After 24 or 48 hours of expression at 28°C, the cells were harvested by centrifugation for 20 minutes at 4500g. The cell pellet was resuspended and washed in 20 mM potassium phosphate buffer, pH 7.4, containing 2% glycerol followed by a centrifugation step. The 2.4 g cell mass was suspended in 100 ml buffer containing 2% glycerol. The substrate (200 µM) and EDTA (20 mM) were added and the cells were incubated for 24 hours at 30°C. The reaction was stopped by adding the same volume of chloroform and extracted as described [20].

HPLC and LC-MS analysis for DOC conversion by CYP260A1

The sample was mixed vigorously and the organic phase was extracted twice with chloroform. The pooled samples were dried in speed-vac and analyzed by HPLC as described [20]. Briefly, the steroids were resuspended in 50% acetonitrile and separated on a Jasco reversed phase HPLC system (Tokyo, Japan) composed of an auto sampler AS-2050 plus, pump PU-2080, gradient mixer LG-2080-02 and an UV-detector UV-2075. A reversed phase column (Nucleodur R100-5 C18ec, particle size 3 µm, length 125 mm, and internal diameter 4 mm, Macherey-Nagel) was used to separate DOC and its products. The separation of the substrate was done by a gradient elution of acetonitrile 10-100% for 15 min and was monitored at 240 nm. The column temperature was kept constant at 40°C with a peltier oven. The sample volume of 20 µl was injected into the HPLC for the analysis. The peaks were identified by using the ChromPass software (V.1.7.403.1, Jasco). Pure steroids (>99%) were used as standards to identify the retention time (t_R) of the peaks on HPLC. For the LC-MS measurement, the HPLC from Water®Alliance®2695 containing diode-array-detector 990 coupled with ESI-MS (Bruker, Germany) was used. For ionization, APCI (atmospheric pressure chemical ionization) was measured in positive mode using the same column and gradient as mentioned earlier.

NMR characterization of the CYP260A1 product

The fractions of the purified product were pooled and dried in a rotary evaporator. The residue was dissolved in $CDCl_3$ for NMR analysis. NMR data were recorded with a Bruker DRX (Rheinstetten, Germany) 500 NMR spectrometer at 300 K at NMR spectroscopy facility (Institut für Pharmazeutische Biologie, Universität des Saarlandes). The chemical shifts were relative to $CHCl_3$ at δ 7.24 (^{1}H NMR) or $CDCl_3$ at δ 77.00 (^{13}C NMR) using the standard δ notation in parts per million (ppm). The 1D NMR (^{1}H and ^{13}C NMR, DEPT135) and the 2D NMR spectra (gs-HH-COSY, gs-NOESY, gs-HSQCED, and gs-HMBC) was recorded using BRUKER pulse program library.

Docking of substrates into the crystal structure of CYP260B1

The automated docking program AUTODOCK (version 4.20) [40, 41] was applied for docking of DOC locally into the substrate free crystal structure of CYP260A1 that we have solved in this study. The Windows version 1.5.6 of Autodock Tools was used to compute Kollman charges for the enzyme CYP260A1 and Gasteiger-Marsili charges for the steroidal-ligands [42]. A partial charge of +0.400e was assigned manually to the heme-iron, which corresponds to Fe(II) that was compensated by adjusting the partial charges of the ligating nitrogen atoms to 0.348e. Flexible bonds of the ligands were assigned automatically and verified by manual inspection. The local docking was performed using a cubic grid box (54×54×54 points with a grid spacing of 0.375 Å) was centered 5 Å above the heme-

iron. For each of the ligands, 100 docking runs were carried out applying the Lamarckian genetic algorithm using default parameter settings.

Results and discussion

Overall crystal structure of CYP260A1

The crystal structure of CYP260A1 in the space group $P3_221$ was solved at 2.67 Å resolution. As a model, the crystal structure of CYP260B1 from *Sorangium cellulosum* So ce56 (PDB entry 5HIW) with a sequence identity of 47% was used [18] for the molecular replacement. The crystal structure of CYP260A1 consisted of four molecules in the asymmetric unit (Figure 1. A). The first 50 amino acid residues were unresolved because of the absence of the electron density in this region and seem to be very flexible. The amino acids were traced at the N-terminus from Met51 in chain B and C, Ser48 in chain A and Asp52 in chain D. At the C-terminus, the electron density until His446 in chains A, B and D, and His445 in chain C was determined. In addition, gaps with lacking electron density were observed at the residue Gly168 in chain A, Pro214-Met215 and Arg241-Asp245 in chain B, and Pro194-Glu196 in chain D. Each of the molecules contains a heme group and water molecules as described in Table 1.

Three chains (A, C and D) of CYP260A1 show a closed conformation with glycerol molecules bound in the active sites. In these chains, the loop between the F-helix and the G-helix covers the access channel which leads from the enzyme surface to the heme center (Figure 1. B). In contrast, only the active site of chain B contains water molecules and differs in the location of the F and G helices compared to the other three chains (Figure 1. C). In addition, the F-G loop is flexible in chain B with no visible electron density and seems to be in open conformation. Such ligand free open and closed conformations have also been reported for P450 PikC from *Streptomyces venezuelae* [43]. Furthermore, it has been observed that the substrate-free P450epoK crystallized in a nearly closed conformation [44] compared with the open form observed for CYP102A1 (P450BM-3) [45] and CYP109B1 from *Bacillus subtilis* [46]. The observed open and close conformations are stabilized by the respective crystal packing forces. The interconversion between these conformations is essential for substrate access to the active site, catalysis, and the subsequent release of the product.

CYP260A1 displays the classic P450 topology consisting of 12 α-helices (A-helix – L-helix) and 8 β-strands (Figure 1. B). The central I-helix runs through the whole molecule with a length of approximately 48 Å. The F-helix and G-helix are projected outside forming the access channel. The heme-iron is bound to the proximal cysteine, Cys390 (2.2 Å distance), and embedded between the distal I-helix and the proximal L-helix. The A- and B-rings of the heme in CYP260A1 show an interaction

with the hydrophobic polypeptide chain with non-polar residues from the D-, I- and L-helices, which is a very common topologic feature of most of the P450s The heme propionate groups are tightly bound to side chains of His131, Arg135, Arg331 and His388, in which the C-ring propionate forms a salt bridge with the side-chain of Arg331 (Figure 1. D) and the D-ring propionate interacts with the N atoms from the side-chains of Arg135, His131 and His388.

The active site of CYP260A1 consists of the residues Phe114, Leu119, Ala124, Leu209, Leu212, Val213, Leu274, Ser275, Leu278, Gly279, Glu282, Thr283, Ser326, Phe327, Leu330 and Val432 (Figure 1. D). In the substrate free crystal structure of CYP260A1, the conserved Thr283 is placed towards the heme-center and forms an acid-alcohol pair with Glu282. This acid-alcohol pair was considered to be involved in the P450 catalysis [47-50]. The residue Glu282 interacts via a hydrogen bond with Arg206. In addition, there is a water molecule coordinated only in the chain B (Figure 1. D). The detailed structural characteristics are listed in Table 1. The structure factors as well as the final coordinates have been deposited in the Protein Data Bank under ID 5LIV.

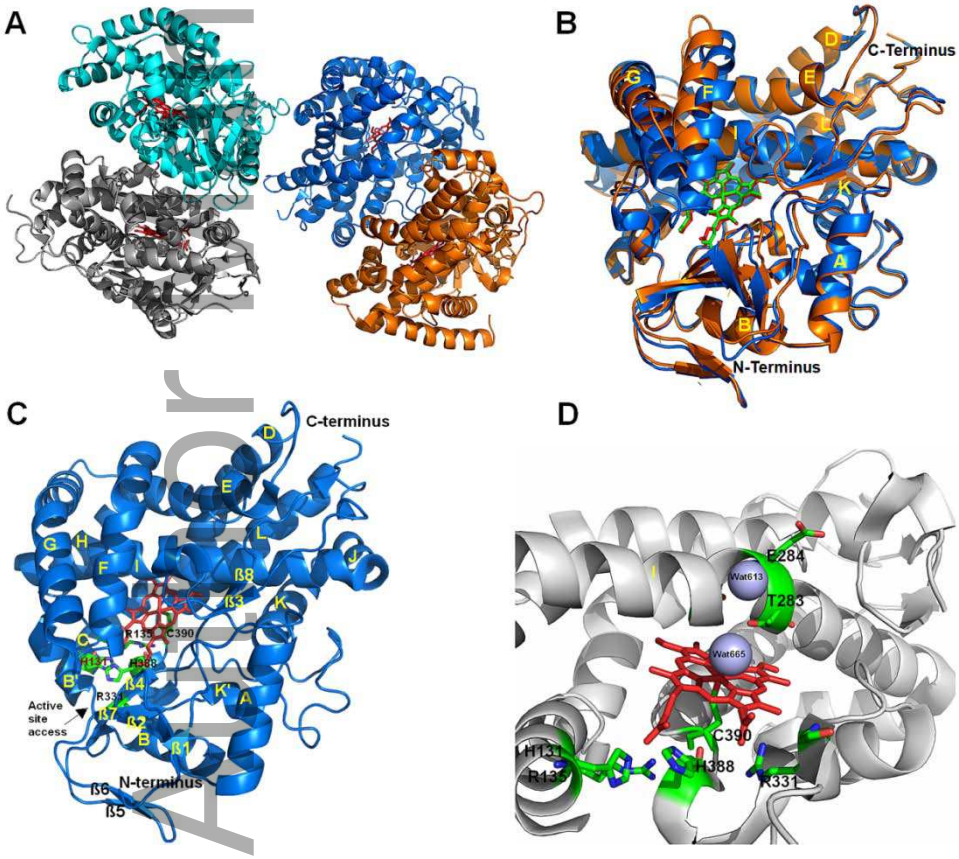

Figure 1. Crystal structure of CYP260A1. A. The four molecules, chain A (cyan), chain B (orange), chain C (blue) and chain D (gray) were found in the asymmetric unit of the substrate free crystal structure of CYP260A1. B. The superimposed structure of the open conformation of chain B (orange) and the close conformation of chain C (blue) is shown. C. The 12α-helices (A-helix – L-helix) and 8β-

strands (β1-β8) in the chain C of CYP260A1 is shown. D. The active site residues of CYP260A1 with the two coordinated water molecules (W613 and W665) (lightblue spheres) are shown.

Table 1: Data collection and refinement statistics of the crystal of CY260A1

PDB entry	5LIV
Beamline	ID14-4 (ESRF, Grenoble)
Space group	$P3_221$ (154)
Unit cell dimensions	
a, b, c [Å]	234.56, 234.56, 96.43
α/β/γ [°]	90/90/120
Wavelength [Å]	0.9393
Resolution of data [Å] [a]	69.93-2.67 (2.72-2.67)
No. of observations [a]	473782 (21277)
No. of unique reflections [a]	86158 (4459)
Completeness [%] [a]	99.7 (97.9)
Redundancy [a]	5.5 (4.8)
$<I/\sigma(I)>$ [a]	4.8 (1.2)
R_{merge} [%] [a]	12.1 (55.5)
R_{meas} [%] [a, b]	14.8 (69.1)
$R_{p.i.m.}$ [%] [a, c]	8.3 (40.6)
CC(1/2) [a]	0.992 (0.764)
Wilson *B* factor [$Å^2$]	40.5
Refinement	
R_{cryst} [d] / R_{free} [e] [%]	18.7/22.3
No. of molecules in the asymmetric unit	4
Residues included in the model (total no. of protein atoms)	1570 (12183)
Water molecules (belonging to chain A/B/C/D)	337 (78/66/117/76)
Ligands	protoporphyrin IX containing Fe, dimethyl sulfoxide (DMSO), glycerol, 2-(N-morpholino)-ethanesulfonic acid (MES), sulfate ion
Overall *B* factor [$Å^2$]	44.0
B Factor for protein chains [$Å^2$]	
overall	40.97

A/B/C/D	47.14/51.88/34.94/44.14
B Factors for ligands [Å^2]	
Waters	33.63
Heme per chain A/B/C/D	26.91/23.70/19.17/24.61
Ramachandran outliers	
Favored [%]	96.6
Allowed [%]	2.9
Outliers [%]	0.5
rmsd for bond lengths [Å]	0.017
rmsd for bond angles [°]	1.920

[a] Values in parentheses are calculated for the highest resolution shell

[b] $R_{meas} = \sum_{\mathbf{h}} \left(\frac{n_h}{n_h-1}\right) \sum_l |I_{hl} - \langle I_{\mathbf{h}}\rangle| \,/\, \sum_{\mathbf{h}} \sum_l \langle I_{\mathbf{h}}\rangle$

[c] $R_{p.i.m.} = \sum_{\mathbf{h}} \left(\frac{1}{n_h-1}\right) \sum_l |I_{hl} - \langle I_{\mathbf{h}}\rangle| \,/\, \sum_{\mathbf{h}} \sum_l \langle I_{\mathbf{h}}\rangle$

[d] $R_{cryst} = 100 \sum \big||F_{obs}| - |F_{calc}|\big| / \sum |F_{obs}|$

[e] Calculation of R_{free} was performed analogous to R_{cryst} excluding 5 % of randomly chosen reflexes

***In vitro* and *in vivo* conversion of DOC by CYP260A1**

Although we have recently shown that CYP260A1 performed the 1α-hydroxylation of C-19 steroids [20], C-21 steroids have never been tested. In this study, DOC, a mineralocorticoid, was used for the conversion of Δ4 C-21 steroids and the characterization of its major product.

The LC-MS measurement of the *in vitro* conversion of DOC ($[M+Z]^+$ = 331.2) showed two main products (peak 4; ~26% and peak 6; ~11%) at a retention time (t_R) of 5.28 min and 7.13 min with $[M+H]^+$ of 347.2 and 329.2 indicating a monohydroxylated product (*Δm/z* of +16), and the formation of either an additional double bond, an epoxide, or a keto group (*Δm/z* of -2), respectively. In addition, 4 side-products corresponding to the peaks 1 (~3% with $[M+Z]^+$ = 363.2), 2 (~2% with $[M+Z]^+$ = 345.2), 3 (~4% with $[M+Z]^+$ = 347.2), and 5 (~2% with $[M+Z]^+$ = 347.2) at t_R of 4.13, 4.41, 5.07, and 6.36 min, respectively, were also obtained during the *in vitro* reaction. The product peak 1 (*Δm/z* of +32), both the peaks 3 and 6 (each having *Δm/z* of +16) and peak 2 (*Δm/z* of +14) indicated double hydroxylation, single hydroxylation, and an addition of a hydroxy-group along with the formation of either a double bond, an epoxide or a keto group, respectively. (Figure 2. A). Steady-state kinetic investigations of the DOC conversion showed a K_m value of 25 ± 4 µM and a catalytic maximum rate of 1.74 ± 0.07 min^{-1} (Figure 2. C).

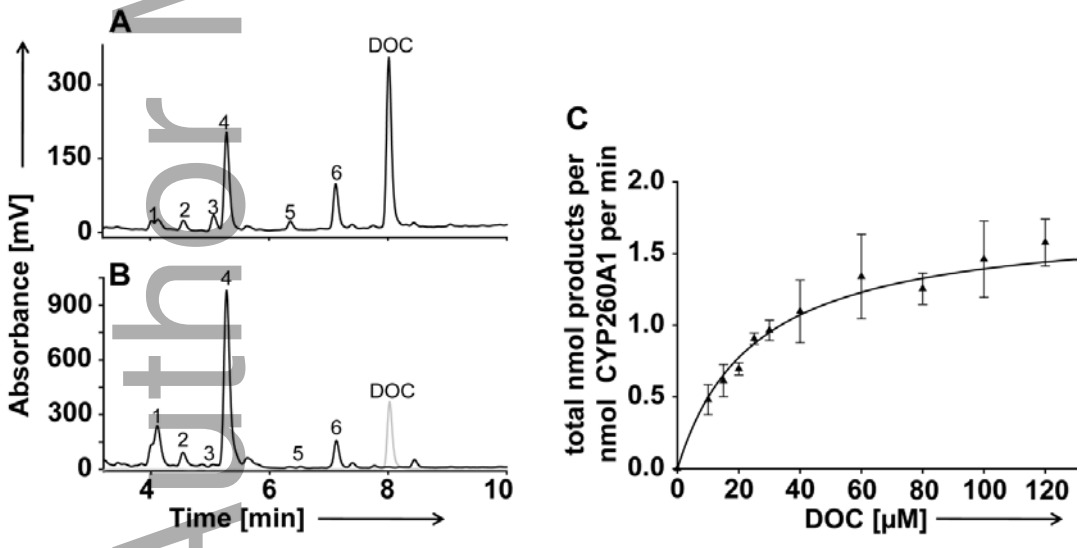

Figure 2. LC-MS chromatogram of the *vitro* (A) and an *E. coli* based whole-cell conversion (B) of DOC by CYP260A1. The activity was reconstituted with the heterologous redox partners Adx and AdR. The ratio of CYP260A1: Adx: AdR was 1: 10: 3. The numbers indicated in the chromatogram represent the product peaks for the conversion of DOC. The major product corresponding to peak 4 was identified as 1α-hydroxylated-11-DOC. C. Kinetic

study of DOC conversion. The error bar in the figures represents the standard deviation of 3–5 independent measurements.

Since we were interested to characterize the major product peak 4, CYP260A1 dependent *E. coli* based whole cell bioconversion of DOC was performed. The *in vivo* conversion of DOC using CYP260A1 and a co-expression of Adx and AdR showed an identical product pattern that has been observed during the *in vitro* reaction (Figure 2. B). Our optimized *E. coli* based whole-cell system was able to produce a high enough yield to purify the major product peak 4 (t_R = 5.28 min, *Δm/z* of +16) and the product was characterized by 1D- and 2D-NMR. The product was identified as 1α-hydroxy-11-deoxycorticosterone (Table 2).

The production of 1α-hydroxylated steroids by chemical means is very challenging. Although a nine-step synthesis of 1α-hydroxytestosterone from dihydrotestosterone [51] as well as the synthesis of 1α-hydroxycorticosterone from corticosterone 21-acetate [52] or a somewhat shorter route from 17β-hydroxyandrosta-1,4-diene-3-one [53] have been reported, the yields of the 1α-hydroxylated products were either very low or a mixture of 1α- and 2α-epoxy derivatives was obtained. In addition, the detection of 1β-hydroxytestosterone either by human liver microsomes or by the recombinant CYP3A4 enzyme has been described. However, the yield is very low and associated with a mixture of other steroidal products. Since the modification at position C-1 of the steroidal A-ring is a pre-requisite to derive some synthetic anabolic steroids like mesterolone and methenolone [54, 55] the explicit production of the 1α-hydroxy derivative of DOC in this study and in our recent study of producing the 1α-hydroxylated products from Δ4 C-19 steroids (testosterone, androstenedione, 11-oxo-androstendione) [20] highlights the biotechnological significance of CYP260A1.

Table 2: NMR data of the main product of CYP260A1-dependent DOC

	1α-hydroxy-11-deoxycorticosterone	
Carbon	**δ_C**	**δ_H (*J* in Hz)**
1	72.04	4.08 *dd* (3.5/3)

2	42.86	2.75 *dd* (17/3) 2.55 *dd* (17/3.5/1)
3	196.41	-
4	123.48	5.79 *dd* (1/1)
5	166.60	-
6	32.84	2.39 *m* 2.36 *m*
7	31.00	1.83 *m* 1.08 *dddd* (13/13/11.5/5.5)
8	35.20	1.56 *ddd* (11.5/11/3.5)
9	44.70	1.70 *m*
10	43.17	-
11	20.32	1.66 *dddd* (11.5/11.5/3.5/3.5) 1.43 *m*
12	38.21	1.93 *m* 1.42 *m*
13	44.67	-
14	56.08	1.24 *m*
15	24.55	1.78 *m* 1.34*m*
16	22.95	2.22 *m* 1.77 *m*
17	59.09	2.46 *dd* (9/9)
18	13.44	0.69 *s* (3H)
19	18.54	1.18 *s* (3H)
20	210.12	-
21	69.42	4.20 *dd* (19/4.5) 4.14 *dd* (19/4)
21-OH	-	3.21 *dd* (4.5/4)

Docking study

Since CYP260A1 was able to produce peak 4 as the major product from the conversion of DOC, we were interested to investigate the structure function relationship for such selectivity. For this, the substrate free crystal structure of CYP260A1 that has been solved in this study was used for docking experiments.

The docking of DOC into the substrate free crystal structure of CYP260A1 showed four different poses (Supplemental Table 1). The frequency of the docking cluster for the pose I is very negligible (only 1%) despite having the lowest energy (-11.29 kcal/mol) compared to the poses II (~38%), III (~21%) and IV (~40%) with the mean binding energy of -10.68, -10.80 and -10.81 kcal/mol, respectively.

In the pose II, the energetically most feasible conformation shows the D-ring of the substrate oriented towards the Ser275 residue (Figure 3. A). In this pose, the 3-keto group at the A-ring of DOC showed a hydrogen bond with Ser326 (~2.092 Å), in addition to a hydrogen bond between the C21 carbonyl group and Ala124 (~2.199 Å). As a result, the substrate was held above the heme-plane giving accesses to the hydroxylation of D- and C-rings, in which the distance from Fe to C14 of the substrate is the shortest (3.736 Å) followed by Fe-C7 (3.764) (Supplemental Table 1, Figure 3. A). Likewise, the pose IV also showed a similar orientation, in which the D-ring of the DOC is closer to the heme-plane (Figure 3. C, Supplemental Table 1) and the active site is

comprised of Phe114, Ser275, Leu278, Gly279, Leu330, Phe327 and Val329 without any hydrogen bond interactions.

However, docking pose III showed a horizontally flipped orientation of the substrate compared to the poses II and IV, in which the 3-keto group of the A-ring of the DOC faced towards the Ser275 residue and displays two hydrogen bonds between C21 carbonyl group and Tyr426 (2.131 Å) as well as Val432 (1.792 Å) (Figure 3. B). In this pose, the active site consists of Leu209, Ser275, Gly279, Leu278, Thr283, Ser326, Phe327, Gly328, Val432 and Tyr426. This orientation of the substrate provides the most feasible hydroxylation position at C-1 (~4.239 Å), which, indeed, is the major product observed throughout the *in vitro* and *in vivo* conversion of DOC as the product peak 4 (*Δm/z* of +16), identified as 1α-hydroxy-11-deoxycorticosterone.

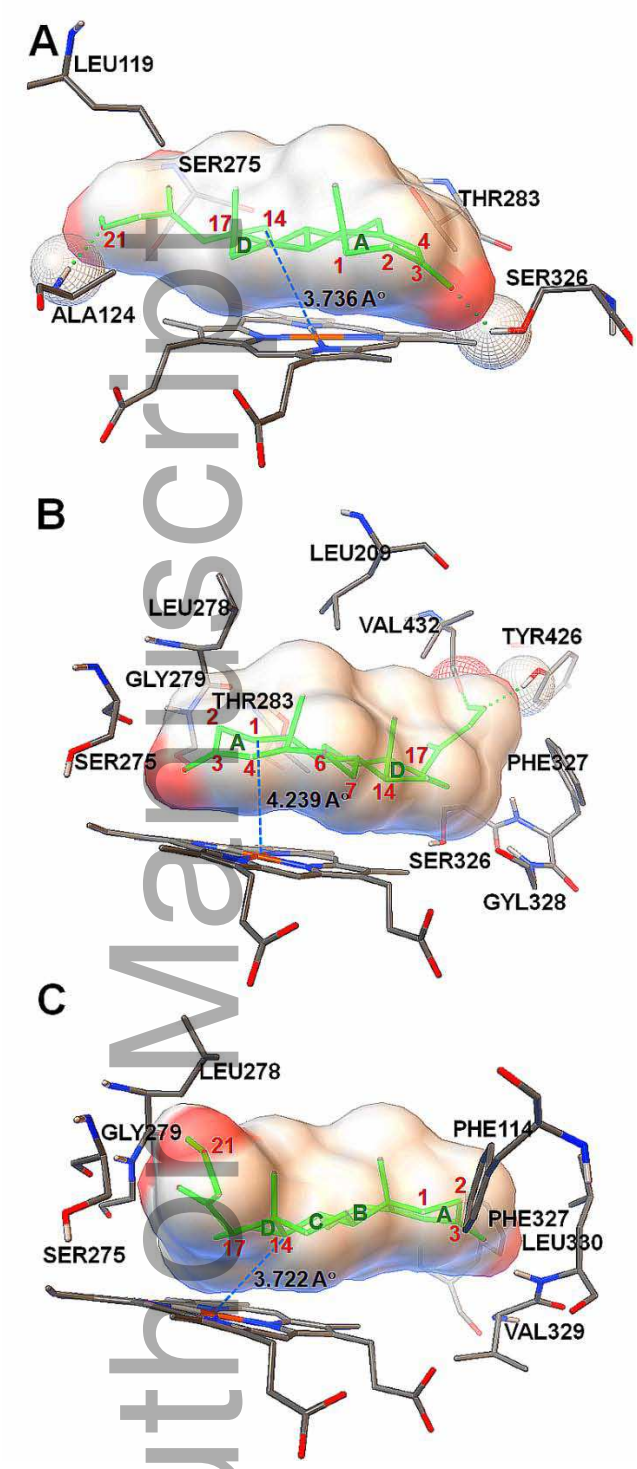

Figure 3: Docking conformations of DOC into the crystal structure of CYP260A1. The docking poses II (A), III (B) and IV (C) are shown. The default program of Autodock version 4.2 was used. The ligand steroid is shown as green stick, surrounded by a molecular surface. The surface is colored with atomic colors in regions that contact the receptor, and gray in regions that are not in contact. The carbon surface is shown in red. The hydrogen bonds (in a wireframed-sphere) are shown in green dotted lines. The most possible hydroxylating C-atoms from the heme-center (blue dashed line) to the DOC are shown. The steroidal rings are

represented by A to D, and the most feasible hydroxylating positions identified by P450s are numbered.

Site directed mutagenesis of CYP260A1

Since in our docking experiment, pose II (Figure 3. A) showed a hydrogen bond between the 3-keto group of DOC at the A-ring with Ser326 leading to less accessibility for the hydroxylation at the position C1 compared with poses III and IV (Supplemental Table S1), we were interested to study the effect of Ser326 onto the catalytic activity and selectivity of DOC conversion. Therefore, in order to disrupt the existing hydrogen bond between the 3-keto group of DOC and S326, we aimed to create a mutant giving more access of DOC to the heme-plane of CYP260A1. Asparagine (Asp/N) which has a carboxamide side chain instead of the hydroxyl group was chosen to replace the Ser326 residue so that the substrate could fit into the active site and could maintain the polarity of the residue. In fact, the mutant S326N showed a 2-fold higher conversion (~95% *vs* ~48%) and ~2-fold better selectivity for peak 4, the 1α-hydroxy-DOC product, compared with the wild type CYP260A1 (~76% vs 26%) (Figure 4).

In addition, the observed docking conformation also showed the possibility to accommodate the substrate or the pre-formed product(s) either having the A- or D-ring closure towards the heme-plane, suggesting the possibility of multiple hydroxylations. Since S326N showed higher activity and selectivity for the product 4 (1α-hydroxylated product) compared with the wild type CYP260A1, it is hypothesized that the absence of the residue Ser326 might have oriented the substrate as observed in docking pose II (Figure 3. B) resulting in the more pronounced production of the product peak 4, the 1α-hydroxy-11-DOC (Figure 4).

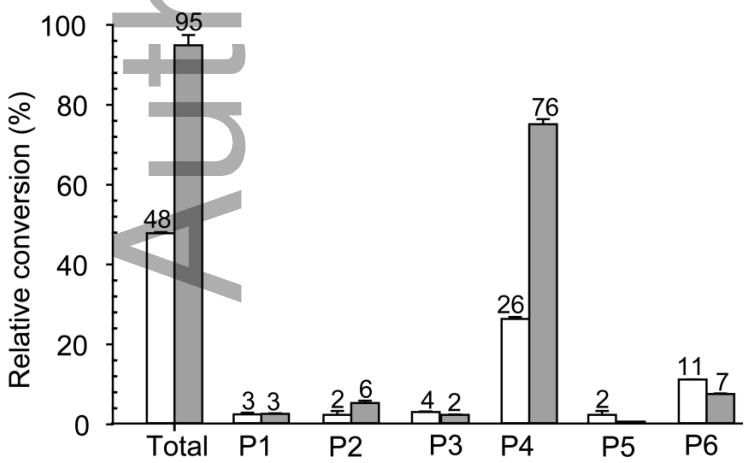

Figure 4: Comparison of the steady state *in vitro* conversion of DOC by wild type CYP260A1 (blank bar) and S326N (grey bar). The products obtained upon the conversion of DOC by the P450s are shown as the product peaks P1-P6. The error bar in the figures represents the standard deviation of 5 independent measurements. The activity was reconstituted with the heterologous redox partners Adx and AdR. The ratio of CYP260A1: Adx: AdR was 1:20:3. The major product corresponding to peak 4 was identified as 1α-hydroxylated-DOC.

In conclusion, the crystal structure of CYP260A1 has been solved for the first time and the structure-function relationship for the conversion of DOC was studied. Since the 1α-hydroxylated product of steroids has a potential pharmaceutical importance, the increase of the selectivity of 1α-hydroxylation by the variant S326N created by engineering the active site of CYP260A1 proves the way to use CYP260A1 also for the derivatization of other steroids and steroidal drugs.

Acknowledgement

This work was supported by a grant from the Deutsche Forschungsgemeinschaft to R.B. (BE 1343/23-1/23-2), grants from the Deutsche Forschungsgemeinschaft (DFG, INST 256/275-1 FUGG and INST 256/299-1 FUGG to CRDL) and the Staatskanzlei Saarland (LFFP 11/02 and 15/04) to CRDL. The authors thank Birgit Heider-Lips for protein purification, and Dr. Josef Zapp for measuring the NMR samples.

Author contributions

YK and RB designed the concept of the project, analyzed and interpreted the results. YK performed the experiments, and MR performed technical contribution for the NMR measurements. YC and CRDL solved the crystal structure. YK performs crystallization and participated in resolution of the crystal structure. All authors read and approved the final manuscript.

References

1. Guengerich FP (2001) Common and Uncommon Cytochrome P450 Reactions Related to Metabolism and Chemical Toxicity. *Chemical Research in Toxicology* **14**, 611-650, doi: 10.1021/tx0002583.
2. Coon MJ (2005) Cytochrome P450: nature's most versatile biological catalyst. *Annu Rev Pharmacol Toxicol* **45**, 1-25.

3. Girvan HM & Munro AW (2016) Applications of microbial cytochrome P450 enzymes in biotechnology and synthetic biology. *Curr Opin Chem Biol* **31**, 136-145.
4. Pateraki I, Heskes AM & Hamberger B (2015) Cytochromes P450 for terpene functionalisation and metabolic engineering. *Adv Biochem Eng Biotechnol* **148**, 107-139.
5. Bernhardt R & Urlacher VB (2014) Cytochromes P450 as promising catalysts for biotechnological application: chances and limitations. *Appl Microbiol Biotechnol* **98**, 6185-6203.
6. Guengerich FP & Munro AW (2013) Unusual cytochrome p450 enzymes and reactions. *J Biol Chem* **288**, 17065-17073.
7. Kelly SL & Kelly DE (2013) Microbial cytochromes P450: biodiversity and biotechnology. Where do cytochromes P450 come from, what do they do and what can they do for us? *Philos Trans R Soc Lond B Biol Sci* **368**, 19.
8. Podust LM & Sherman DH (2012) Diversity of P450 enzymes in the biosynthesis of natural products. *Nat Prod Rep* **29**, 1251-1266.
9. Hannemann F, Bichet A, Ewen KM & Bernhardt R (2007) Cytochrome P450 systems--biological variations of electron transport chains. *Biochim Biophys Acta* **3**, 330-344.
10. Guengerich FP, Waterman MR & Egli M (2016) Recent Structural Insights into Cytochrome P450 Function. *Trends in Pharmacological Sciences* **37**, 625-640, doi: http://dx.doi.org/10.1016/j.tips.2016.05.006.
11. Kiss FM, Khatri Y, Zapp J & Bernhardt R (2015) Identification of new substrates for the CYP106A1-mediated 11-oxidation and investigation of the reaction mechanism. *FEBS Lett* **589**, 2320-2326.
12. Schmitz D, Zapp J & Bernhardt R (2014) Steroid conversion with CYP106A2 - production of pharmaceutically interesting DHEA metabolites. *Microb Cell Fact* **13**, 1475-2859.
13. Virus C & Bernhardt R (2008) Molecular evolution of a steroid hydroxylating cytochrome P450 using a versatile steroid detection system for screening. *Lipids* **43**, 1133-1141.
14. Ouellet H, Guan S, Johnston JB, Chow ED, Kells PM, Burlingame AL, Cox JS, Podust LM & de Montellano PR (2010) Mycobacterium tuberculosis CYP125A1, a steroid C27 monooxygenase that detoxifies intracellularly generated cholest-4-en-3-one. *Mol Microbiol* **77**, 730-742.

15. Johnston JB, Singh AA, Clary AA, Chen CK, Hayes PY, Chow S, De Voss JJ & Ortiz de Montellano PR (2012) Substrate analog studies of the omega-regiospecificity of Mycobacterium tuberculosis cholesterol metabolizing cytochrome P450 enzymes CYP124A1, CYP125A1 and CYP142A1. *Bioorg Med Chem* **20**, 4064-4081.
16. Garcia-Fernandez E, Frank DJ, Galan B, Kells PM, Podust LM, Garcia JL & Ortiz de Montellano PR (2013) A highly conserved mycobacterial cholesterol catabolic pathway. *Environ Microbiol* **15**, 2342-2359.
17. Herzog K, Bracco P, Onoda A, Hayashi T, Hoffmann K & Schallmey A (2014) Enzyme-substrate complex structures of CYP154C5 shed light on its mode of highly selective steroid hydroxylation. *Acta Crystallogr D Biol Crystallogr* **70**, 2875-2889.
18. Salamanca-Pinzon SG, Khatri Y, Carius Y, Keller L, Muller R, Lancaster CR & Bernhardt R *Structure-function analysis for the hydroxylation of Delta4 C21-steroids by the myxobacterial CYP260B1*. FEBS Lett. 2016 Jun;590(12):1838-51. doi: 10.1002/1873-3468.12217. Epub 2016 Jun 3.
19. Kuzikov AV, Masamrekh RA, Khatri Y, Zavialova MG, Bernhardt R, Archakov AI & Shumyantseva VV (2016) Scrutiny of electrochemically-driven electrocatalysis of C-19 steroid 1alpha-hydroxylase (CYP260A1) from Sorangium cellulosum So ce56. *Anal Biochem* **513**, 28-35.
20. Khatri Y, Ringle M, Lisurek M, von Kries JP, Zapp J & Bernhardt R (2016) Substrate Hunting for the Myxobacterial CYP260A1 Revealed New 1alpha-Hydroxylated Products from C-19 Steroids. *Chembiochem* **17**, 90-101.
21. Pradella S, Hans A, Sproer C, Reichenbach H, Gerth K & Beyer S (2002) Characterisation, genome size and genetic manipulation of the myxobacterium Sorangium cellulosum So ce56. *Arch Microbiol* **178**, 484-492.
22. Gaitatzis N, Kunze B & Muller R (2005) Novel insights into siderophore formation in myxobacteria. *Chembiochem* **6**, 365-374.
23. Khatri Y, Hannemann F, Ewen KM, Pistorius D, Perlova O, Kagawa N, Brachmann AO, Muller R & Bernhardt R (2010) The CYPome of Sorangium cellulosum So ce56 and identification of CYP109D1 as a new fatty acid hydroxylase. *Chem Biol* **17**, 1295-1305.
24. Ewen KM, Hannemann F, Khatri Y, Perlova O, Kappl R, Krug D, Huttermann J, Muller R & Bernhardt R (2009) Genome mining in Sorangium cellulosum So ce56: identification and characterization of the homologous electron transfer proteins of a myxobacterial cytochrome P450. *J Biol Chem* **284**, 28590-28598.

25. Schifrin A, Litzenburger M, Ringle M, Ly TT & Bernhardt R (2015) New Sesquiterpene Oxidations with CYP260A1 and CYP264B1 from Sorangium cellulosum So ce56. *Chembiochem* **16**, 2624-2632.
26. Litzenburger M, Kern F, Khatri Y & Bernhardt R (2015) Conversions of tricyclic antidepressants and antipsychotics with selected P450s from Sorangium cellulosum So ce56. *Drug Metab Dispos* **43**, 392-399.
27. Ringle M, Khatri Y, Zapp J, Hannemann F & Bernhardt R (2013) Application of a new versatile electron transfer system for cytochrome P450-based Escherichia coli whole-cell bioconversions. *Appl Microbiol Biotechnol* **97**, 7741-7754.
28. Sagara Y, Wada A, Takata Y, Waterman MR, Sekimizu K & Horiuchi T (1993) Direct Expression of Adrenodoxin Reductase in Escherichia coli and the Functional Characterization. *Biological & Pharmaceutical Bulletin* **16**, 627-630, doi: 10.1248/bpb.16.627.
29. Uhlmann H, Kraft R & Bernhardt R (1994) C-terminal region of adrenodoxin affects its structural integrity and determines differences in its electron transfer function to cytochrome P-450. *Journal of Biological Chemistry* **269**, 22557-22564.
30. Muller FG & Lancaster CR (2013) Crystallization of membrane proteins. *Methods Mol Biol*, 487-486_485.
31. Incardona MF, Bourenkov GP, Levik K, Pieritz RA, Popov AN & Svensson O (2009) EDNA: a framework for plugin-based applications applied to X-ray experiment online data analysis. *Journal of Syncrotron Radiation* **16**, 872-879.
32. Leslie AG (2006) The integration of macromolecular diffraction data. *Acta Crystallogr D Biol Crystallogr* **62**, 48-57.
33. Evans P (2006) Scaling and assessment of data quality. *Acta Crystallogr D Biol Crystallogr* **62**, 72-82.
34. Collaborative Computational Project N (1994) The CCP4 suite: programs for protein crystallography. *Acta crystallographica Section D Biological Crystallography* **D50**, 760-763.
35. Vagin A & Teplyakov A (1997) MOLREP: an Automated Program for Molecular Replacement. *Journal of Applied Crystallography* **30**, 1022-1025, doi: doi:10.1107/S0021889897006766.
36. Vagin A & Teplyakov A (2010) Molecular replacement with MOLREP. *Acta Crystallogr D Biol Crystallogr* **66**, 22-25.

37. Emsley P & Cowtan K (2004) Coot: model-building tools for molecular graphics. *Acta crystallographica Section D Biological Crystallography* **D60**, 2126-2132.
38. Murshudov GN, Vagin AA & Dodson EJ (1997) Refinement of macromolecular structures by the maximum-likelihood method. *Acta crystallographica Section D Biological Crystallography* **D53**, 240-255.
39. Omura T & Sato R (1964) The Carbon Monoxide-Binding Pigment of Liver Microsomes. Ii. Solubilization, Purification, and Properties. *J Biol Chem* **239**, 2379-2385.
40. Huey R, Morris GM, Olson AJ & Goodsell DS (2007) A semiempirical free energy force field with charge-based desolvation. *Journal of Computational Chemistry* **28**, 1145-1152, doi: 10.1002/jcc.20634.
41. Morris GM, Goodsell DS, Halliday RS, Huey R, Hart WE, Belew RK & Olson AJ (1998) Automated docking using a Lamarckian genetic algorithm and an empirical binding free energy function. *Journal of Computational Chemistry* **19**, 1639-1662, doi: 10.1002/(sici)1096-987x(19981115)19:14<1639::aid-jcc10>3.0.co;2-b.
42. Sanner MF (1999) Python: a programming language for software integration and development. *J Mol Graph Model* **17**, 57-61.
43. Sherman DH, Li S, Yermalitskaya LV, Kim Y, Smith JA, Waterman MR & Podust LM (2006) The structural basis for substrate anchoring, active site selectivity, and product formation by P450 PikC from Streptomyces venezuelae. *J Biol Chem* **281**, 26289-26297.
44. Nagano S, Li H, Shimizu H, Nishida C, Ogura H, de Montellano PRO & Poulos TL (2003) Crystal Structures of Epothilone D-bound, Epothilone B-bound, and Substrate-free Forms of Cytochrome P450epoK. *Journal of Biological Chemistry* **278**, 44886-44893, doi: 10.1074/jbc.M308115200.
45. Ravichandran KG, Boddupalli SS, Hasermann CA, Peterson JA & Deisenhofer J (1993) Crystal structure of hemoprotein domain of P450BM-3, a prototype for microsomal P450's. *Science* **261**, 731-736.
46. Zhang A, Zhang T, Hall EA, Hutchinson S, Cryle MJ, Wong LL, Zhou W & Bell SG (2015) The crystal structure of the versatile cytochrome P450 enzyme CYP109B1 from Bacillus subtilis. *Mol Biosyst* **11**, 869-881.
47. Khatri Y, Gregory MC, Grinkova YV, Denisov IG & Sligar SG (2014) Active site proton delivery and the lyase activity of human CYP17A1. *Biochem Biophys Res Commun* **443**, 179-184.

48. Makris TM, von Koenig K, Schlichting I & Sligar SG (2007) Alteration of P450 distal pocket solvent leads to impaired proton delivery and changes in heme geometry. *Biochemistry* **46**, 14129-14140.
49. Raag R, Martinis SA, Sligar SG & Poulos TL (1991) Crystal structure of the cytochrome P-450CAM active site mutant Thr252Ala. *Biochemistry* **30**, 11420-11429.
50. Vidakovic M, Sligar SG, Li H & Poulos TL (1998) Understanding the role of the essential Asp251 in cytochrome p450cam using site-directed mutagenesis, crystallography, and kinetic solvent isotope effect. *Biochemistry* **37**, 9211-9219.
51. Mann J & Pietrzak B (1989) Synthesis of 1-α-hydroxytestosterone. *Tetrahedron* **45**, 1549-1552, doi: http://dx.doi.org/10.1016/0040-4020(89)80153-X.
52. Kime DE (1975) Synthesis of 1alpha-hydroxycorticosterone. *J Chem Soc Perkin* **1**, 2371-2374.
53. Garside D, Kirk DN & Waldron NM (1994) Synthesis of hydroxylated steroid hormones via conjugate addition of a silyl-cuprate reagent. *Steroids* **59**, 702-711.
54. Petrow V (1996) A history of steroid chemistry: some contributions from European industry. *Steroids* **61**, 473-475.
55. Schänzer W & Donike M (1993) Metabolism of anabolic steroids in man: synthesis and use of reference substances for identification of anabolic steroid metabolites. *Analytica Chimica Acta* **275**, 23-48, doi: http://dx.doi.org/10.1016/0003-2670(93)80274-O.

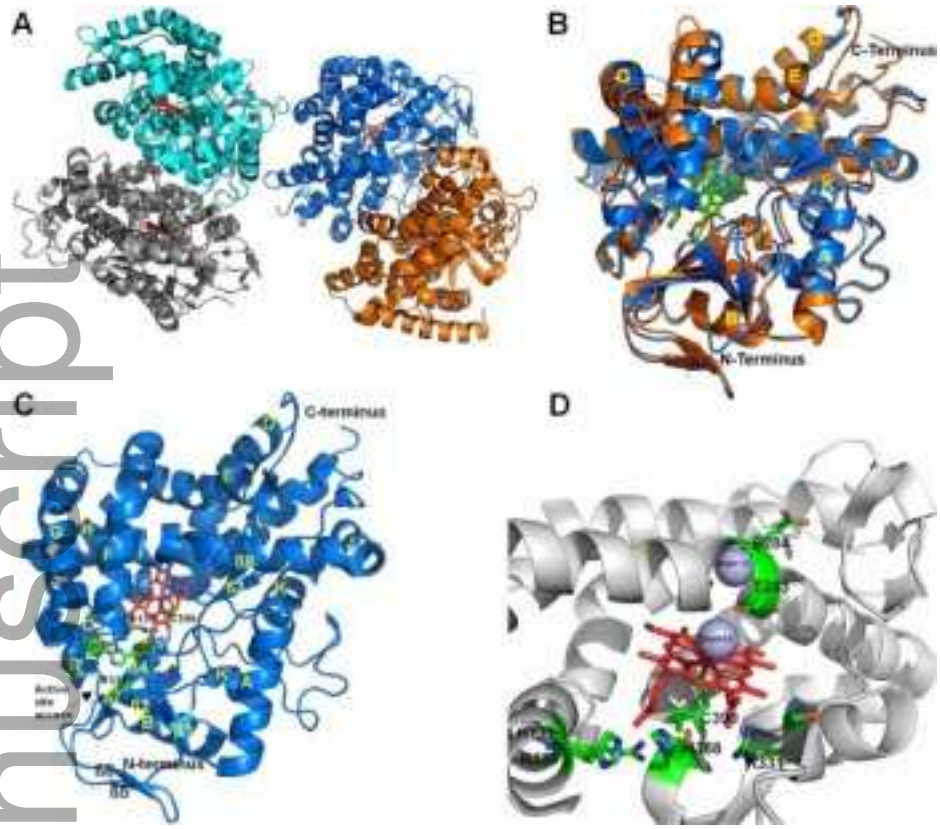

feb2_12479_f1.tif

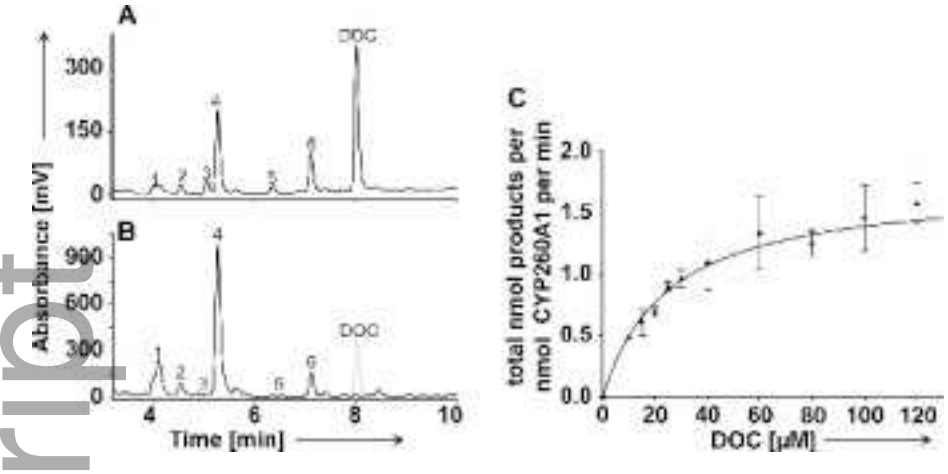

feb2_12479_f2.tif

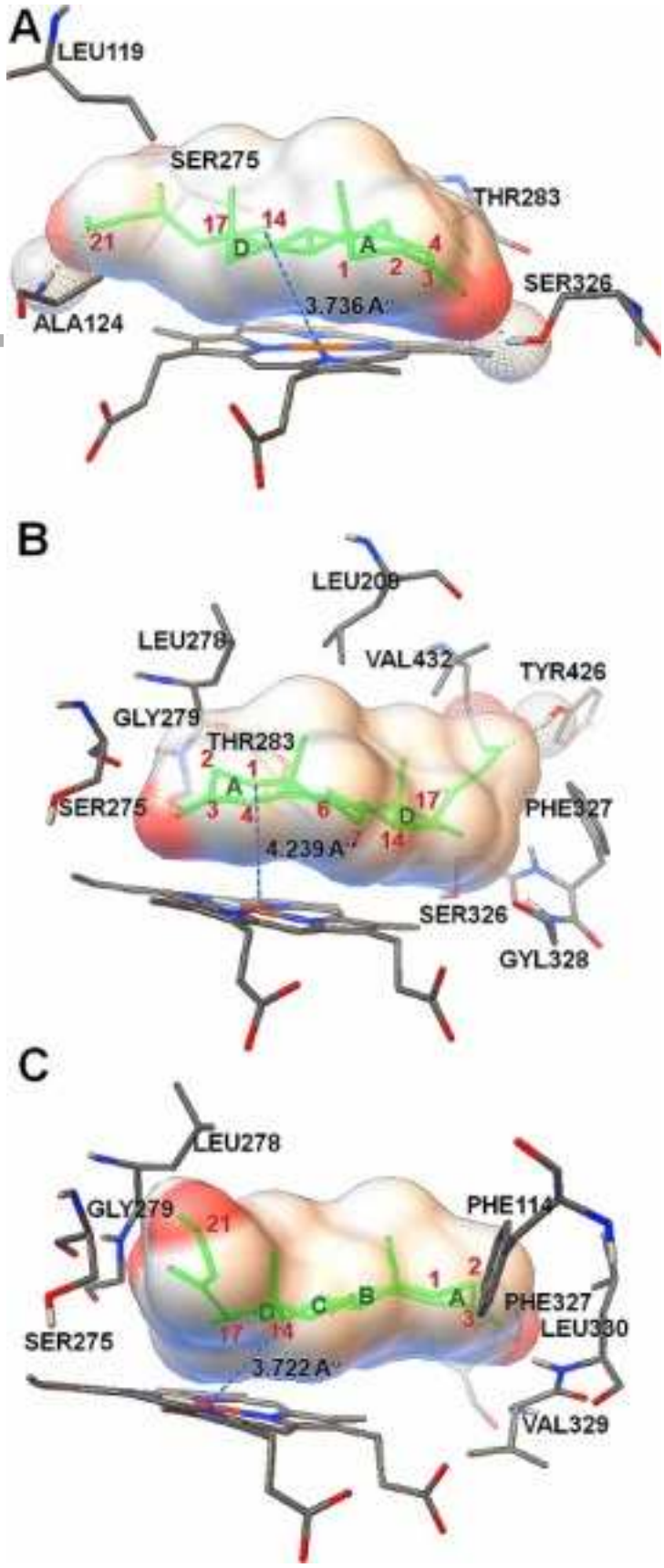

feb2_12479_f3.tif

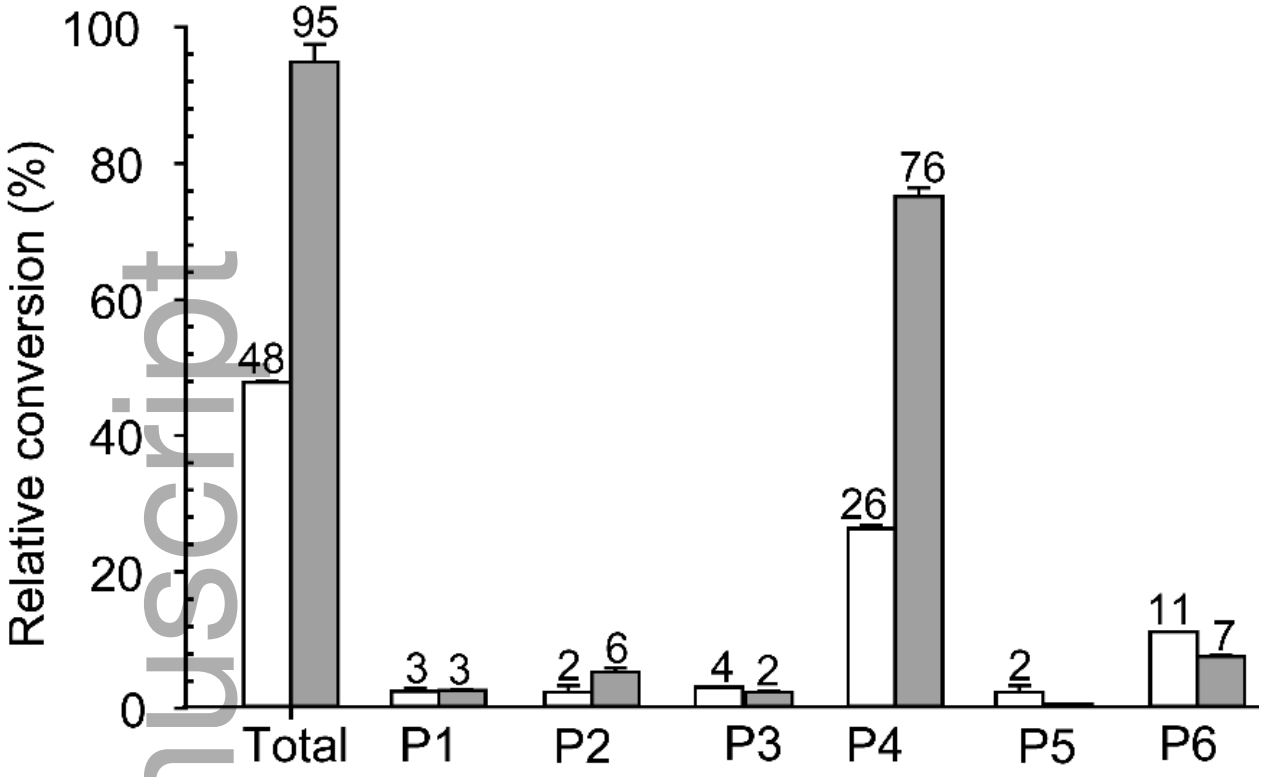

feb2_12479_f4.tif